4996 *Inorg. Chem.* **2010**, *49*, 4996–5002
DOI: 10.1021/ic100099w

Inorganic Chemistry
Article

Low-Temperature Coprecipitation Synthesis and Luminescent Properties of $LaPO_4:Ln^{3+}$ (Ln^{3+} = Ce^{3+}, Tb^{3+}) Nanowires and $LaPO_4:Ce^{3+},Tb^{3+}/LaPO_4$ Core/Shell Nanowires

Mei Yang,[†,‡] Hongpeng You,[*,†] Kai Liu,[†,‡] Yuhua Zheng,[†,‡] Ning Guo,[†,‡] and Hongjie Zhang[*,†]

[†]*State Key Laboratory of Rare Earth Resource Utilization, Changchun Institute of Applied Chemistry, Chinese Academy of Sciences, Changchun 130022, People's Republic of China, and* [‡]*Graduate University of the Chinese Academy of Sciences, Beijing 100049, People's Republic of China*

Received January 17, 2010

$LaPO_4:Ln^{3+}$ (Ln^{3+}= Ce^{3+}, Tb^{3+}) and $LaPO_4:Ce^{3+},Tb^{3+}/LaPO_4$ core/shell nanowires have been synthesized on a large scale through a direct precipitation in a water-based system under moderate conditions without the assistance of any surfactant, catalyst, or template. The diameters of the obtained nanowires are about 15 nm, and the lengths range from a few hundred nanometers to several micrometers. The influences of the solution acidity, reaction time, and proportion of ethanol to water on the final products were investigated in detail. It was found that the lengths of nanowires can be efficiently controlled by adjusting the reaction conditions. The formation mechanism of the products is proposed on the basis of time-dependent experiments as well as the crystal structure of the products. The luminescent properties of the products were also studied. A $LaPO_4$ shell on the $LaPO_4:Ce^{3+},Tb^{3+}$ nanowires can greatly increase the intensity of the product, and the thickness of the shell also has an important effect on the intensity of the product. The method is a novel and facile route for the synthesis of one-dimensional lanthanide phosphates.

1. Introduction

Recently, one-dimensional (1D) nanostructures such as wires, rods, belts, and tubes have become the focus of intensive research because they are expected to play an important role in both interconnectors and functional units for the fabrication of nanodevices of electronics, optoelectronics, and biochemical sensing.[1−6] Among the 1D nanomaterials, nanowires have played key roles in the fabrication of these nanodevices.[2,3,7]

As an important sort of phosphors, lanthanide-doped nanomaterials have formed a class of highly luminescent materials that display narrow emission bands as well as long luminescence decay times in the range of milliseconds, which may have potential applications in transparent luminescence layers, luminescence fillers in transparent matrices, fluorescence resonance energy transfer (FRET) assays, biolabeling, optical imaging, biomedical applications, and so on.[8−19] Among these lanthanide inorganic salts, rare earth (RE) orthophosphates ($REPO_4$) have been widely used in the production of luminescence or laser materials, moisture sensors,

*To whom correspondence should be addressed. Tel.: 86431- 85692798. Fax: 86431-85698041. E-mail: hpyou@ciac.jl.cn (H.Y.) or hongjie@ciac.jl.cn (H.Z.).

(1) Wang, Z. J. *Adv. Mater.* **2000**, *12*, 1295.
(2) Xia, Y. N.; Yang, P. D.; Sun, Y. G.; Wu, Y. Y.; Mayers, B.; Gates, B.; Yin, Y. D.; Kim, F.; Yan, H. Q. *Adv. Mater.* **2003**, *15*, 353.
(3) Hu, J. T.; Odom, T. W.; Lieber, C. M. *Acc. Chem. Res.* **1999**, *32*, 435.
(4) Wu, Y. Y.; Yan, H. Q.; Huang, M.; Messer, B.; Song, J. H.; Yang, P. D. *Chem.—Eur. J.* **2002**, *8*, 1260.
(5) Partzke, G. R.; Krumeich, F.; Nesper, R. *Angew. Chem., Int. Ed.* **2002**, *41*, 2446.
(6) Li, X. Y.; Zhao, F. H.; Fu, J. X.; Yang, X. F.; Wang, J.; Liang, C. L.; Wu, M. M. *Cryst. Grow. Des.* **2009**, *9*, 409.
(7) Duan, X. F.; Hang, Y.; Agarwal, R.; Lieber, C. M. *Nature* **2003**, *421*, 241.
(8) Song, Y. H.; You, H. P.; Yang, M.; Zheng, Y. H.; Liu, K.; Jia, G.; Huang, Y. J.; Zhang, L. H.; Zhang, H. J. *Inorg. Chem.* **2010**, *49*, 1674.
(9) Dubertret, B.; Skouride, P.; Norris, D. J.; Noireaus, V.; Brivanlou, A. H.; Libchaber, A. *Science* **2002**, *298*, 1759.
(10) Li, Y. J.; Yan, B. *Inorg. Chem.* **2009**, *48*, 8276.
(11) Li, Q.; Yam, V. W. W. *Angew. Chem., Int. Ed.* **2007**, *46*, 3486.
(12) Karmaoui, M.; Mafra, L.; Sá Ferreira, R. A.; Rocha, J.; Carlos, L. D.; Pinna, N. *J. Phys. Chem. C* **2007**, *111*, 2539.
(13) Wang, F.; Xue, X.; Liu, X. *Angew. Chem., Int. Ed.* **2008**, *47*, 906.
(14) Li, G. C.; Chao, K.; Peng, H. R.; Chen, K. Z.; Zhang, Z. K. *J. Phys. Chem. C* **2008**, *112*, 16452.
(15) Pellegrino, T.; Kudera, S.; Liedl, T.; Javier, A. M.; Manna, L.; Parak, W. *Small* **2005**, *1*, 48.
(16) Zhang, C. Y.; Yeh, H. C.; Kuroki, M. T.; Wang, T. H. *Nat. Mater.* **2005**, *4*, 826.
(17) Jia, G.; Liu, K.; Zheng, Y. H.; Song, Y. H.; You, H. P. *Cryst. Growth Des.* **2009**, *9*, 3702.
(18) Buissette, V.; Moreau, M.; Gacoin, T.; Boilot, J. P.; Ching, J. Y. C.; Mercier, T. L. *Chem. Mater.* **2004**, *16*, 3767.
(19) Lehmann, O.; Kömpe, K.; Haase, M. *J. Am. Chem. Soc.* **2004**, *126*, 14935.
(20) Riwotzki, K.; Meyssamy, H.; Kornowski, A.; Haase, M. *J. Phys. Chem. B* **2000**, *104*, 2824.
(21) Schuetz, P.; Caruso, F. *Chem. Mater.* **2002**, *14*, 4509.
(22) Meiser, F.; Cortez, C.; Caruso, F. *Angew. Chem., Int. Ed.* **2004**, *43*, 5954.

 Published on Web 05/12/2010

heat-resistant materials, and nuclear waste disposal,[20,21] due to their high chemical stability, high quantum yield, and low toxicity.[22] At the same time, it has also been found that the quantum yield of nanomaterials is usually lower than that of the corresponding bulk materials because of the numerous defects on the surface of nanomaterials. A proper shell of an undoped material around each nanomaterial can efficiently confine the excitation to the core and eliminate nonradiative relaxation pathways. Recently, monazite-type $CePO_4$:Tb/$LaPO_4$ core/shell nanoparticles with 70% PL quantum yield have been synthesized by a liquid-phase synthesis in high-boiling point coordinating solvents, and $CePO_4$:Tb/$LaPO_4$ core/shell nanowires have been synthesized using hydrothermal methods.[23,24]

Up to now, many synthesis methodologies have been employed for the synthesis of nanowires including templates, ligand control, and oriented attachment.[25,26] For the synthesis of 1D $LnPO_4$ nanowires, hydrothermal synthesis was often used, and few reports were focused on 1D $LnPO_4$ nanowires or $LnPO_4$ core/shell nanowires prepared using direct precipitation in a water-based system under moderate conditions.[24,27−29] Compared with the hydrothermal method, solution-based direct precipitation syntheses possess some advantages, such as inexpensive facilities, low reaction temperatures, safe reaction processes, easily controllable reaction conditions, low production cost, and a large amount of product. Furthermore, compared with the synthesis in the organic solvents, a water-based system would provide a relatively green chemical alternative to prepare various nanomaterials because it does not involve toxic organic solvents. For these reasons, the water-based systems as a more attractive route for the shape-controlled synthesis of nanomaterials have recently received more and more attention.

In this paper, we present a new example of the synthesis of highly uniform $LaPO_4$:Ln^{3+} (Ln^{3+} = Ce^{3+}, Tb^{3+}) and $LaPO_4$:Ce^{3+},Tb^{3+}/$LaPO_4$ core/shell nanowires. The novelties of our study include mainly the following aspects: (i) Our method is used to synthesize lanthanide phosphate nanowires and core/shell nanowires for the first time. (ii) Our method offers a facile, green, and low-cost route to synthesize $LaPO_4$:Ln^{3+} (Ln^{3+} = Ce^{3+}, Tb^{3+}) and $LaPO_4$:Ce^{3+},Tb^{3+}/$LaPO_4$ core/shell nanowires on a large scale without using any surfactant, catalyst, or template during the synthesis process.

2. Experimental Section

La_2O_3 (99.999%), Tb_4O_7 (99.999%), and $Ce(NO_3)_3\cdot 6H_2O$ were purchased from Wuxi Yiteng Rare-Earth Limited Corporation. All of the other analytical grade reagents were purchased from Beijing Chemical Corporation and used as received without further purification.

2.1. Synthesis of $Ln(NO_3)_3\cdot 6H_2O$. $La(NO_3)_3\cdot 6H_2O$, $La_{0.55}Ce_{0.45}(NO_3)_3\cdot 6H_2O$, $La_{0.85}Tb_{0.15}(NO_3)_3\cdot 6H_2O$, and $La_{0.4}Ce_{0.45}Tb_{0.15}(NO_3)_3\cdot 6H_2O$ were obtained by dissolving La_2O_3, Tb_4O_7, and $Ce(NO_3)_3\cdot 6H_2O$ with exact compositions (stoichiometry) and amounts in a dilute HNO_3 solution under heating with agitation and subsequently were evaporated until the desired products were obtained.

2.2. Synthesis of $LaPO_4$:Ln^{3+} (Ln^{3+} = Ce^{3+}, Tb^{3+}) Nanowires. In a typical synthesis, 2 mmol of $La_{0.55}Ce_{0.45}(NO_3)_3\cdot 6H_2O$ (or $La_{0.85}Tb_{0.15}(NO_3)_3\cdot 6H_2O$ or $La_{0.4}Ce_{0.45}Tb_{0.15}(NO_3)_3\cdot 6H_2O$) was dissolved in deionized water. An ethanol−water solution containing 3 mmol of $(NH_4)_2HPO_4\cdot 12H_2O$ was then added into the above solution (the amounts of ethanol range from 0 to 20 mL). The pH value of the obtained solution was adjusted by using HNO_3 (the amounts of HNO_3 range from 2 to 4 mL). The obtained transparent solution was subsequently transferred into a 100 mL round flask and maintained at different temperatures (30−100 °C) for a certain time (2 min to 7.5 h; reflux conditions were used for the reaction at 100 °C). After cooling to room temperature naturally, the precipitate was collected and washed with deionized water and ethanol several times. The final products were dried at 60 °C for 12 h in the air.

2.3. Synthesis of $LaPO_4$:Ce^{3+},Tb^{3+}/$LaPO_4$ and $LaPO_4$:Ce^{3+},Tb^{3+}/$LaPO_4$:Ce^{3+},Tb^{3+} Core/Shell Nanowires. The synthesis of the $LaPO_4$:Ce^{3+},Tb^{3+} nanowires was the same as the above, but maintained at 90 °C for 5 h. A quarter of the obtained $LaPO_4$:Ce^{3+},Tb^{3+} product was dispersed into a $La(NO_3)_3$ (or $La(NO_3)_3$:Ce^{3+},Tb^{3+}) aqueous solution by vigorous sonicating for 15 min, and the resulting suspension changed into a cream-colored colloidal solution. The ethanol−water solution containing $(NH_4)_2HPO_4$ was added into the above solution under stirring, and the pH value of the obtained suspension solution was subsequently adjusted by using corresponding amounts of HNO_3. Then, the obtained colloidal solution was transferred into a 100 mL round flask and maintained at 90 °C for another 5 h. After cooling to room temperature naturally, the precipitate was collected and washed with deionized water and ethanol several times. The final products were dried at 60 °C for 12 h in the air.

2.4. Characterizations. XRD patterns were measured by a Rigaku-D X-ray powder diffractometer with Cu Kα radiation (λ = 1.5418 Å). The morphology of the samples was inspected using a field emission scanning electron microscope (HITACHI S-4800). TEM images were collected on a TF20 Transmission Electron Microscope (TEM) operating at an accelerating voltage of 200 kV. Excitation and emission spectra were recorded with a HITACHI F-4500 fluorescence spectrophotometer equipped with a 150 W xenon lamp as the excitation source.

3. Results and Discussion

Figure 1 shows the XRD patterns of the $LaPO_4$:Ce^{3+} samples obtained at different temperatures for 7.5 h. When the reaction temperature was lower than 90 °C, all the diffraction peaks could be readily indexed to the hexagonal phase of $LaPO_4$ (JCPDS card 75-1881); no additional peaks of other phases have been found. As the temperature was increased to 100 °C, the peaks of monoclinic phase of $LaPO_4$ could be observed. All of the diffraction peaks are apparently broadened because of the small size of the nanowires.

Figure 2 shows the SEM images of the $LaPO_4$:Ce^{3+} samples obtained at different temperatures for 7.5 h. It can be found that the reaction temperature has an important effect on the length of the nanowires. When the reaction temperature was lower than 90 °C, the length of the obtained nanowires increased with the temperature. When the reaction temperature was controlled at 90 °C, the products were composed of superlong nanowires. Their diameters are about 10 nm, and their lengths range from a few hundred nanometers to several micrometers. However, as the reaction temperature was increased to 100 °C, the length of the

(23) Kompe, K.; Borchert, H.; Storz, J.; Lobo, A.; Adam, S.; Moller, T.; Haase, M. *Angew. Chem. Int.Ed.* **2003**, *42*, 5513.
(24) Fang, Y. P.; Xu, A. W.; Dong, W. F. *Small* **2005**, *1*, 967.
(25) Wyrwa, D.; Beyer, N.; Schmid, G. *Nano Lett.* **2002**, *2*, 419.
(26) Cademartiri, L.; Ozin, G. A. *Adv. Mater.* **2009**, *21*, 1013.
(27) Li, Z. Y.; Yin, Y.; Xia, Y. *Appl. Phas. Lett.* **2001**, *78*, 2431.
(28) Zhang, Y. W.; Yan, Z. G.; You, L. P.; Si, R.; Yan, C. H. *Eur. J. Inorg. Chem.* **2003**, *22*, 4099.
(29) Yan, R. X.; Sun, X. M.; Wang, X.; Peng, Q.; Li, Y. D. *Chem.—Eur. J.* **2005**, *11*, 2187.

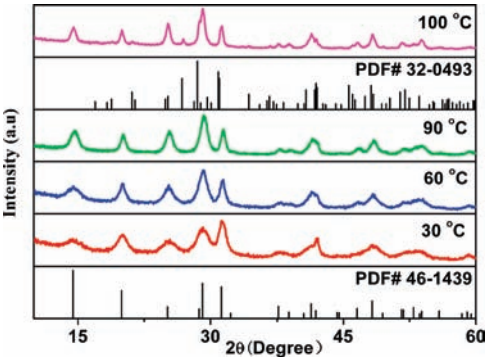

Figure 1. XRD patterns of the $LaPO_4:Ce^{3+}$ nanowires obtained at different temperatures for 7.5 h.

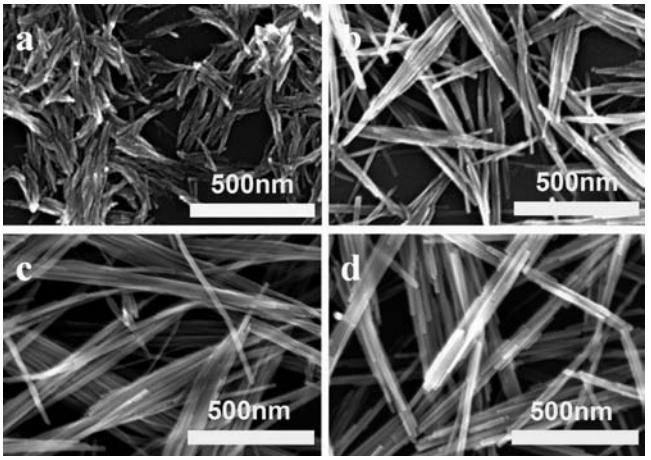

Figure 2. SEM images of the $LaPO_4:Ce^{3+}$ samples obtained at different temperatures for 7.5 h. (a, 30 °C; b, 60 °C; c, 90 °C; d, 100 °C).

nanowires became short and nonuniform due to the phase conversion.

The introduction of different lanthanide ions has little effect on the phase structures of the products. The XRD patterns of the $LaPO_4:Ce^{3+}$, $LaPO_4:Tb^{3+}$, and $LaPO_4:Ce^{3+}$, Tb^{3+}obtained at 90 °C for 7.5 h (Figure S1) illustrate that all of the diffraction peaks can be readily indexed to the hexagonal phase of $LaPO_4$, indicating that the other lanthanide ions have been effectively doped into the hexagonal phase of the $LaPO_4$ host lattice. The corresponding SEM images illustrate that all of the products are composed of superlong nanowires, their diameters are about 10 nm, and the lengths range from a few hundred nanometers to several micrometers (Figure 3). At the same time, it is noted that the lengths of these nanowires change with the variation of the doped lanthanide ions. Figure 3d exhibits the energy dispersive X-ray spectrum (EDX) of $LaPO_4:Ce^{3+},Tb^{3+}$, confirming the presence of La, Ce, Tb, P, and O in the product (Si from the Si substrate).

The outgrowth of a $LaPO_4$ shell on the $LaPO_4:Ce^{3+},Tb^{3+}$ core nanowires also has little effect on the phase structure of the products. The XRD patterns of the $LaPO_4:Ce^{3+},Tb^{3+}$ and $LaPO_4:Ce^{3+},Tb^{3+}/LaPO_4$ core/shell nanowires obtained with different concentrations of $LaPO_4$ indicate that these products also have the same hexagonal phase of $LaPO_4$ (Figure S2, Supporting Information). This result reveals no qualitative difference in structure between the nanowires and the core/shell nanowires. However, the narrowed XRD peaks

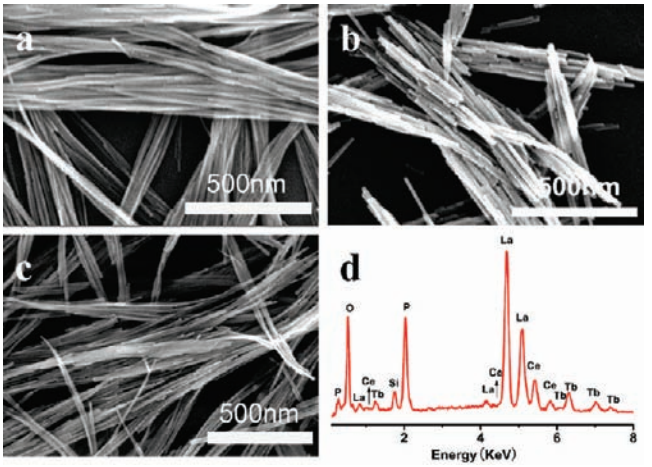

Figure 3. SEM images of the different lanthanide-ion -doped $LaPO_4:Ln^{3+}$ nanowires prepared at 90 °C for 7.5 h (a, $LaPO_4:Ce^{3+}$; b, $LaPO_4:Tb^{3+}$; c, $LaPO_4:Ce^{3+},Tb^{3+}$) and EDX pattern of $LaPO_4:Ce^{3+},Tb^{3+}$ (d).

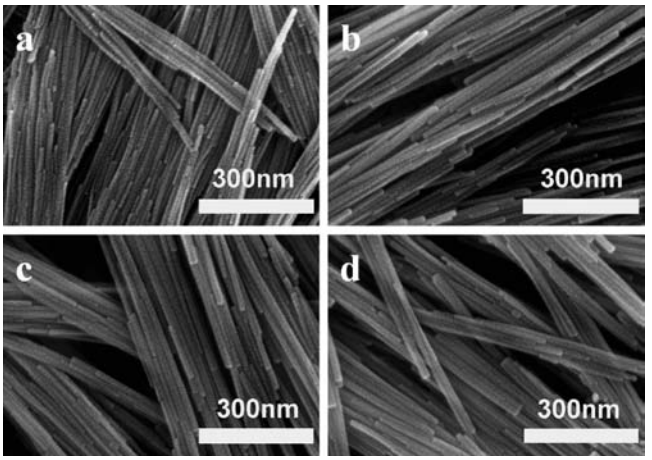

Figure 4. SEM images of the $LaPO_4:Ce^{3+},Tb^{3+}$ nanowires (a) and $LaPO_4:Ce^{3+},Tb^{3+}/LaPO_4$ core/shell nanowires with different concentrations of $LaPO_4$ (b, 0.1 mol/L; c, 0.2 mol/L; d, 0.3 mol/L).

with the increase of the concentration of $LaPO_4$ may indicate the formation of $LaPO_4:Ce^{3+},Tb^{3+}/LaPO_4$ core/shell nanostructures in a certain way. To further confirm the formation of $LaPO_4:Ce^{3+},Tb^{3+}/LaPO_4$ core/shell nanostructures, the SEM images were acquired. Figure 4 shows the SEM images of the $LaPO_4:Ce^{3+},Tb^{3+}$ and $LaPO_4:Ce^{3+},Tb^{3+}/LaPO_4$ core/shell nanowires obtained with different concentrations of $LaPO_4$. It can be observed from the images that the diameter of the products increases with the increase of the concentration of $LaPO_4$. When the concentration of $LaPO_4$ was increased to 0.3 mol/L, the diameter of the obtained nanowires was about double that of the core nanowires (Figure 4a), confirming the successful outgrowth of a shell on the core nanowires of the $LaPO_4:Ce^{3+},Tb^{3+}$.

The $LaPO_4:Ce^{3+}$ nanowires obtained at 90 °C for 5 h and $LaPO_4:Ce^{3+},Tb^{3+}/LaPO_4$ core/shell nanowires with 0.3 mol/L $LaPO_4$ are further characterized by TEM, HRTEM, and a fast Fourier transform pattern (FFT), as shown in Figure 5. The TEM image of the $LaPO_4:Ce^{3+}$ nanowires further confirms the observation in the above SEM image (Figure 5a). A typical HRTEM image of $LaPO_4:Ce^{3+}$ nanowires shows resolved (001) and (100) planes (Figure 5b). The (001) planes are oriented perpendicular to the nanowire growth axis,

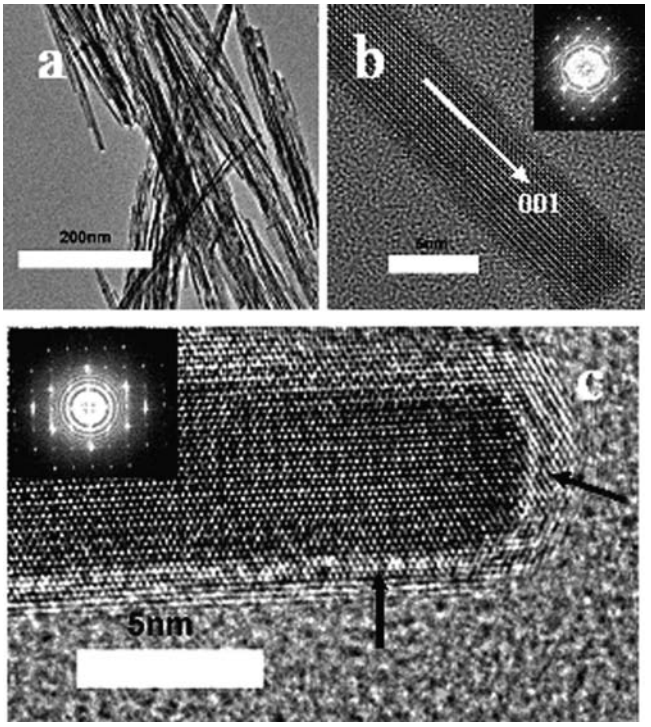

Figure 5. TEM (a), HRTEM images and FFT patterns of the $LaPO_4$:Ce^{3+},Tb^{3+} nanowires obtained at 90 °C for 5 h (b) and $LaPO_4$:Ce^{3+},Tb^{3+}/$LaPO_4$ core/shell nanowires with 0.3 mol/L $LaPO_4$ (c).

indicating the direction of nanowire growth is along the *c* axis. The HRTEM image of $LaPO_4$:Ce^{3+},Tb^{3+}/$LaPO_4$ core/shell nanowires (Figure 5c) confirms the successfully outgrowth of a shell on the core nanowires, as indicated by the black arrow. From the image, it can be found that the distribution of the thickness of the shell is not uniform. The thickness is about 2 nm at the top of the nanorods, but it becomes thin at the other parts, which can be explained by the preferred growth direction along the *c* axis. The lattice fringes are continuous from the core to the shell, indicating that the growth of the $LaPO_4$ shell on the surface of the $LaPO_4$:Ce^{3+}, Tb^{3+}core nanowires appears to be epitaxially coherent. The corresponding fast Fourier transform (FFT) pattern (inset Figure 5b,c) further demonstrates that the as-synthesized nanowires are of a well-crystallized hexagonal $LnPO_4$ single crystal.

In order to understand the formation of different lengths of the $LaPO_4$:Ln^{3+} (Ln^{3+} = Ce^{3+}, Tb^{3+}) nanowires, the nanowires of $LaPO_4$, $CePO_4$, and $TbPO_4$ were prepared under the same reaction conditions. Their XRD patterns (Figure S3, Supporting Information) indicate that they possess the same hexagonal phase of $LnPO_4$. The SEM images of the products (Figure 6) exhibit that their diameters are similar, but their lengths are obviously different. Among the three samples, the length of the $CePO_4$ nanowires is longest, while that of the $TbPO_4$ nanowires is shortest. This result is consistent with the length variation tendency of the $LaPO_4$:Ce^{3+}, $LaPO_4$:Tb^{3+}, and $LaPO_4$:Ce^{3+},Tb^{3+} nanowires, indicating that the introduction of different rare earth ions can affect the crystal growth.

The influential factors on the growth of the $LaPO_4$:Ln^{3+} nanowires were also investigated in detail. First, the solution acidity has an important effect on the morphology of the products. The XRD patterns of the products obtained with

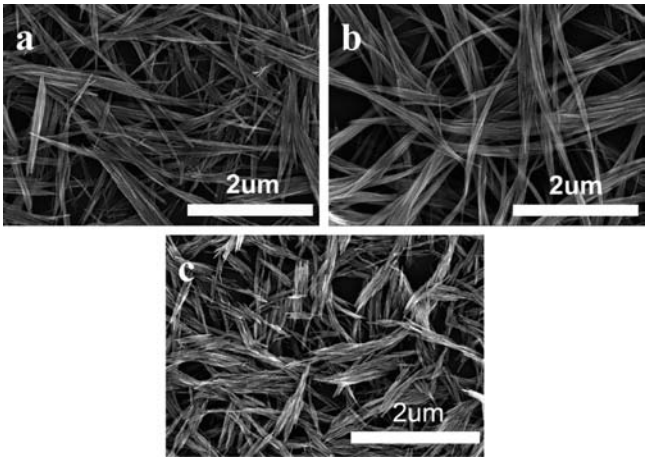

Figure 6. SEM images of $LnPO_4$ samples (a, $LaPO_4$; b, $CePO_4$; c, $TbPO_4$).

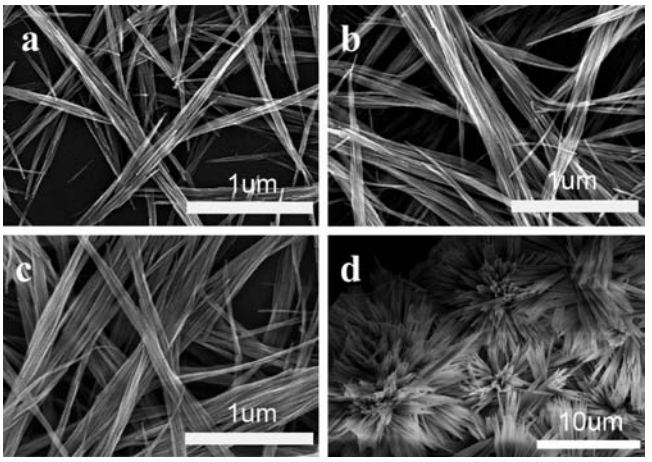

Figure 7. SEM images of the $LaPO_4$:Ce^{3+} samples obtained at 90 °C for 7.5 h with different amounts of concentrated HNO_3 (a, 2 mL; b, 2.5 mL; c, 3.5 mL; d, 4 mL.).

different amounts of HNO_3 (Figure S4, Supporting Information) indicate that the phase structure of the products has no change with the variations of the amounts of HNO_3. The SEM images (Figure 7) display that the change of the amount of HNO_3 has an important influence on the length as well as the aggregation morphology of nanowires. When the content of HNO_3 was 2 mL, the length of the obtained nanowires was nonuniform (Figure 7a). With an increase of the amount of HNO_3, the lengths of the nanowires increased and became uniform (Figure 7b,c). As the content of HNO_3 was further increased to 4 mL, the length of the nanowires increased dramatically and assembled together (Figure 7d).

Second, the amount of ethanol added into the solution also played an important role in controlling the final morphologies of the products. Figure 8 shows the SEM images of the $LaPO_4$:Ce^{3+} samples obtained at 90 °C for 7.5 h with different amounts of ethanol. It can be found that the length of the obtained nanowires increased with the amount of ethanol being lower than 10 mL. As the amount of ethanol further increased to 15 mL, the nanowires became short again and aggregated together to form bundles. The XRD patterns (Figure S5, Supporting Information) reveal that the phase structures of the obtained nanowires do not change with the variation of the amount of ethanol.

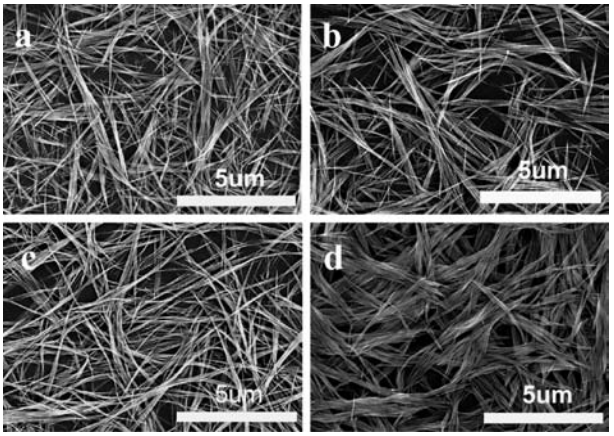

Figure 8. SEM images of $LaPO_4:Ce^{3+}$ samples obtained at 90 °C for 7.5 h with different amounts of ethanol (a, 0 mL; b, 5 mL; c, 10 mL; d, 15 mL.).

In order to investigate the growth mechanism of the nanowires, the time-dependent experiments were further performed. Figure 9 exhibits the SEM images of the nanowires gathered at different reaction times. When the reaction time is only 2 min, small nanorods are obtained (Figure 9a). The length of the nanorods increases, while their diameter changes little with the increase of the reaction time (Figure 9b, c). The length of the nanowires increases to 500 nm as the reaction time is prolonged to 30 min (Figure 9d). The length of the nanowires increases continually to several micrometers, while their diameters still remain at about 15−20 nm with prolonging the reaction time (Figure 9e,f). This result indicates that the length of the nanowires can be efficiently controlled by adjusting the reaction time.

On the basis of the above experimental results and analysis, this surfactant/ligand-free exclusive anisotropic growth of nanowires first can be understood from the viewpoint of the intrinsic structure of hexagonal $LaPO_4$, which is inner 1D infinite linear chains. Viewing along the *a* axis, one can find that the crystal structure of hexagonal $LaPO_4$ can be described as infinite linear chains parallel to the *c* axis (Figure S6, Supporting Information). Meanwhile, the activation energy of the growth at the *c* axis direction is lower than that at the direction perpendicular to the *c* axis direction from a thermodynamic perspective.[30] These imply a higher growth rate along the *c* axis and a lower one perpendicular to the *c* axis. It is the structural feature that plays an important role in the highly preferential growth along the *c* axis to form one-dimensional nanowires. Furthermore, the strong pH-dependent relation with the lengths and the aggregation of the nanowires is due to the sensitive influence of the pH on the solute concentrations ($[Ln^{3+}]$ and $[PO_4^{3-}]$), which suggests that the 1D growth stage was rightly captured by maintaining the solute concentrations in the correct range through the control of the pH. This obvious 1D growth stage observed here is also in agreement with the previous model proposed by Yu et al. and Peng and Peng[31−33] Therefore, we can concluded that the promotion of the anisotropic growth of nanowires in this surfactant/ligand-free system is mainly

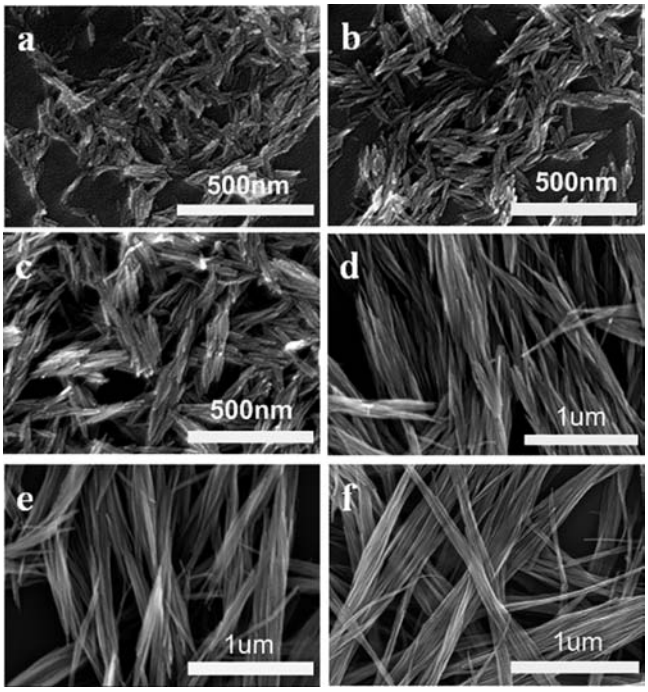

Figure 9. SEM images of the $LaPO_4:Ce^{3+}$ samples obtained at 90 °C with different reaction times (a, 2 min; b, 4 min; c, 8 min; d, 30 min; e, 60 min; f, 7.5 h.).

governed by a general cooperation effect, including the intrinsic structure features, the local solution details, and so on. According to the time-dependent experiments, the growth progress of the nanowires is speculated. At the beginning of the reaction, nuclei were produced in the solution; these nuclei grew into nanowires in the subsequent growth progress.

Figure 10a shows the excitation and emission spectra of the $LaPO_4:Ce^{3+}$. The excitation spectrum shows a broad band centered at 278 nm, which corresponds to the transitions from the ground state $^2F_{5/2}$ to excited 5d states of the Ce^{3+} ions. The emission spectrum exhibits a strong ultraviolet broad band centered at 344 nm, which is due to the 5d → 4f transitions of the Ce^{3+} ions.[34,35] The excitation spectrum of the $LaPO_4:Tb^{3+}$ monitored with the $^5D_4 \rightarrow {}^7F_5$ transition consists of two strong bands and several weak bands from the UV to visible regions (Figure 10b). The strong band at about 225 nm is ascribed to the spin allowed transition, while the weak band at about 260 nm is due to the spin-forbidden transition of the Tb^{3+} ions. The remaining weak sharp bands are assigned to the intra-$4f^8$ transitions from the $^7F_6$ to $^5F_{5,4}$, $^5H_{7-4}$, $^5D_{1,0}$, $^5L_{10-7}$, $^5G_{6-2}$, and $^5D_{2-4}$ levels of the Tb^{3+} ions.[36] The emission spectrum under 260 nm excitation consists of four bands located at about 489, 543, 583, and 620 nm. The four bands are attributed to the $^5D_4 \rightarrow {}^7F_J$ ($J = 6$, 5, 4, 3) transitions of the Tb^{3+} ions, respectively. The excitation spectrum of the $LaPO_4:Ce^{3+},Tb^{3+}$ monitored at 543 nm consists of the strong excitation bands of the Ce^{3+} ions and weak excitation bands of the Tb^{3+} ions (Figure 10c), revealing that the Tb^{3+} ions are essentially excited through

(30) Murphy, K. E.; Altman, M. B.; Wunderlich, B. *J. Appl. Phys.* **1977**, *48*, 4122.
(31) Yu, S. H.; Liu, B.; Mo, M. S.; Huang, J. H.; Liu, X. M.; Qian, Y. T. *Adv. Funct. Mater.* **2003**, *13*, 939.
(32) Peng, Z. A.; Peng, X. G. *J. Am. Chem. Soc.* **2001**, *123*, 1389.
(33) Peng, Z. A.; Peng, X. G. *J. Am. Chem. Soc.* **2002**, *124*, 3343.
(34) Yang, M.; You, H. P.; Zheng, Y. H.; Liu, K.; Jia, G.; Song, Y. H.; Huang, Y. J.; Zhang, L. H.; Zhang, H. J. *Inorg. Chem.* **2009**, *48*, 11559.
(35) Kömpe, K.; Lehmann, O.; Haase, M. *Chem. Mater.* **2006**, *18*, 4442.
(36) Yang, M.; You, H. P.; Song, Y. H.; Huang, Y. J.; Jia, G.; Liu, K.; Zheng, Y. H.; Zhang, L. H.; Zhang, H. J. *J. Phys. Chem. C* **2009**, *113*, 20173.

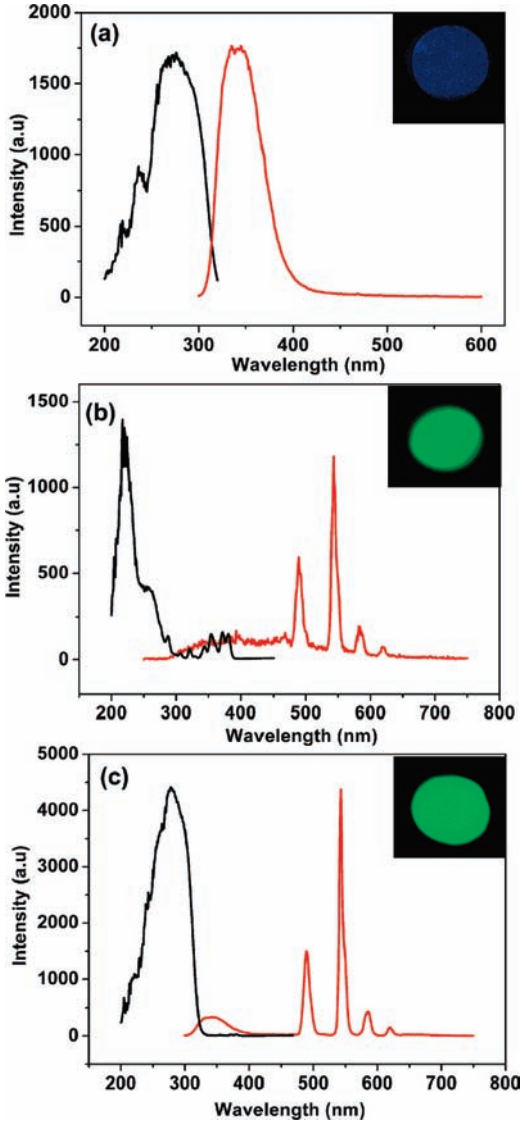

Figure 10. Excitation and emission spectra of the $LaPO_4:Ln^{3+}$ samples obtained at 90 °C for 7.5 h (a, $LaPO_4:Ce^{3+}$; b, $LaPO_4:Tb^{3+}$; c, $LaPO_4:Ce^{3+},Tb^{3+}$; all the measurements of the spectra were operated under the same conditions).

the Ce^{3+} ions. In fact, several weak f−f excitation bands of the Tb^{3+} ions are just present in the region of the Ce^{3+} emission. Thus, the energy transfer from the Ce^{3+} to Tb^{3+} ions occurs.[37] The emission spectrum of the $LaPO_4:Ce^{3+},Tb^{3+}$ contains both a weak emission band of the Ce^{3+} ions and strong green emission bands of the Tb^{3+} ions, indicating that the energy transfer from the Ce^{3+} to Tb^{3+} ions is highly efficient because the emission peak of the Ce^{3+} ions in this host matches well with the f−f absorptions of the Tb^{3+} ions. This result is similar to that observed in the bulk powder materials.[38,39] Comparing with the emission intensity of the $LaPO_4:Tb^{3+}$, one can find that the emission intensity of the $LaPO_4:Ce^{3+},Tb^{3+}$ increases dramatically.

Figure 11 shows the emission spectra of the $LaPO_4:Ce^{3+},Tb^{3+}$ nanowires and $LaPO_4:Ce^{3+},Tb^{3+}/LaPO_4$ core/shell

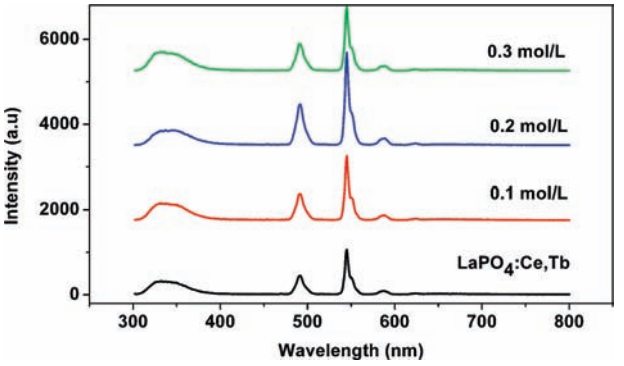

Figure 11. Emission spectra of the $LaPO_4:Ce^{3+},Tb^{3+}$ nanowires and $LaPO_4:Ce^{3+},Tb^{3+}/LaPO_4$ core/shell nanowires obtained with different concentrations of $LaPO_4$ (all the measurements of the spectra were operated under the same conditions).

nanowires with different concentrations of $LaPO_4$. From the spectra, it can be found that the growth of a $LaPO_4$ shell on the $LaPO_4:Ce^{3+},Tb^{3+}$ nanowires can efficiently increase the emission intensity of the products. In general, radiative mechanisms compete with nonradiative mechanisms. Luminescence of nanomaterials often depends on radiative relaxation from a higher state excited to a ground state of rare earth ions, while the surface is most often associated with nonradiative recombination and quenching of the luminescent mechanisms because it deviates from the typically ordered crystal structure including atomic arrangement, composition, surface topography, adsorbed gas, defects, and so on. These changes can greatly decrease the emission intensity of the nanophosphors by nonradiative mechanisms in luminescence processes.[40−42] In our case, the Ce^{3+} and Tb^{3+} ions in the $LaPO_4:Ce^{3+},Tb^{3+}$ nanowires can be divided into two types: one is at the surface of the nanowires, and the other is in the "bulk". The structures of these surface Ce^{3+} and Tb^{3+} ions deviate from the typically ordered crystal structure. This change gives rise to the formation of different kinds of defects surrounding the Ce^{3+} and Tb^{3+} ions, which generate luminescent quenching centers. When the $LaPO_4$ shell was outgrown on the $LaPO_4:Ce^{3+},Tb^{3+}$ nanowires, the $LaPO_4:Ce^{3+},Tb^{3+}$ core nanowires increased, some surface Ce^{3+} and Tb^{3+} ions went into the "bulk" of the nanowires, and the defects of the surrounding Ce^{3+} and Tb^{3+} ions decreased. These changes reduce the nonradiative pathways and suppress the luminescence quenching in the energy-transfer process. As a result, the emission intensity of the $LaPO_4:Ce^{3+},Tb^{3+}/LaPO_4$ core/shell nanowires increases. From the spectra, it also can be observed that the thickness of the shell also has an important influence on the intensity of the products. When the thickness of the shell was kept in a certain range, the emission intensity of the $LaPO_4:Ce^{3+},Tb^{3+}$ increased with the thickness of the shell, but when the thickness was out of this range, the emission intensity decreased again, due to the shell of the $LaPO_4$ inhabiting the absorption of the inner $LaPO_4:Ce^{3+},Tb^{3+}$.

Figure 12 gives the emission spectra of the $LaPO_4:Ce^{3+},Tb^{3+}/LaPO_4$ core/shell nanowire and $LaPO_4:Ce^{3+},Tb^{3+}/LaPO_4:Ce^{3+},Tb^{3+}$ core/shell nanowires. One can note that

(37) Chen, G. Z.; Sun, S. X.; Zhao, W.; Xu, S. L.; You, T. *J. Phys. Chem. C* **2008**, *112*, 20217.
(38) Meyssamy, H.; Riwotzki, K.; Kornowski, A.; Naused, S.; Haase, M. *Adv. Mater.* **1999**, *11*, 840.
(39) Bourcet, J. C.; Fong, F. K. *J. Chem. Phys.* **1974**, *60*, 34.
(40) Abrams, B. L.; Holloway, P. H. *Chem. Rew.* **2004**, *104*, 5783.
(41) Sudarsan, V.; van Veggel, F. C. J. M.; Herring, R. A.; Raudsepp, M. *J. Mater. Chem.* **2005**, *15*, 1332.
(42) Zheng, Y. H.; You, H. P.; Jia, G.; Liu, K.; Song, Y. H.; Yang, M; Zhang, H. J. *Cryst. Growth Des.* **2009**, *9*, 5101.

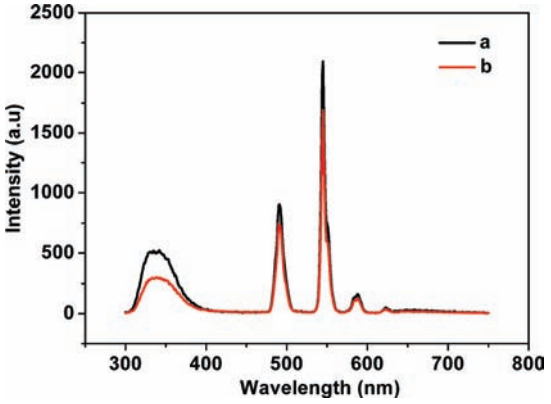

Figure 12. Emission spectra of the $LaPO_4:Ce^{3+},Tb^{3+}/LaPO_4$ core/shell nanowires (a) and $LaPO_4:Ce^{3+},Tb^{3+}$/ $LaPO_4:Ce^{3+},Tb^{3+}$ nanowires (b) obtained under the same reaction conditions (all the measurements of the spectra were operated under the same conditions).

the luminescent intensity of $LaPO_4:Ce^{3+},Tb^{3+}/LaPO_4$ core/shell nanowires is indeed higher than that of $LaPO_4:Ce^{3+}$, Tb^{3+}/ $LaPO_4:Ce^{3+},Tb^{3+}$ core/shell nanowires. This result further supports that the $LaPO_4$ shell grew on the $LaPO_4:Ce^{3+},Tb^{3+}$ core nanowires, as the surface Ce^{3+} and Tb^{3+} ions can go into the "bulk" of the $LaPO_4:Ce^{3+},Tb^{3+}/LaPO_4$ core/shell nanowire when the shell of $LaPO_4$ is outgrown.

4. Conclusion

In summary, we have successfully synthesized super-long $LaPO_4:Ln^{3+}$ (Ln^{3+} = Ce^{3+}, Tb^{3+}) nanowires and $LaPO_4:Ce^{3+},Tb^{3+}/LaPO_4$ core/shell nanowires through a direct precipitation in a water-based system under moderate conditions without any surfactant, catalyst, or template. The diameters of the nanowires are about 15 nm. The lengths of nanowires can be efficiently controlled by adjusting the reaction times, which range from a few hundred nanometers to several micrometers. The HRTEM image of $LaPO_4:Ce^{3+},Tb^{3+}/LaPO_4$ core/shell nanowires confirms the successful outgrowth of the shell on the core nanowires. The influences of the solution acidity, reaction time, and proportion of ethanol to water on the final products have been explored. The formation mechanism of the products is due to the inner crystal structure of the hexagonal $LaPO_4$ and high chemical potential of unique facets. The emission intensity of the $LaPO_4:Ce^{3+},Tb^{3+}$ nanowires is stronger than that of the $LaPO_4:Tb^{3+}$ nanowires, due to the efficient energy transfer from the Ce^{3+} to Tb^{3+} ions. The obtained $LaPO_4:Ce^{3+},Tb^{3+}$ nanowires show strong green luminescence. Moreover, the growth of the $LaPO_4$ shell on $LaPO_4:Ce^{3+},Tb^{3+}$ nanowires can further increase the emission intensity, which may have a potential application in nanodevices of electronics, optoelectronics, and biochemical sensing.

Acknowledgment. This work is financially supported by the National Natural Science Foundation of China (Grant No. 20771098), the Fund for Creative Research Groups (Grant No. 20921002), and the National Basic Research Program of China (973 Program, Grant Nos. 2007CB935502 and 2006CB601103).

Supporting Information Available: XRD patterns of $LaPO_4:Ln^{3+}$ (Ln^{3+} = Ce^{3+}, Tb^{3+}) nanowires (Figure S1); XRD patterns of $LaPO_4:Ce^{3+},Tb^{3+}$ and the $LaPO_4:Ce^{3+},Tb^{3+}/LaPO_4$ core/shell nanowires obtained with different concentrations of $LaPO_4$ (Figure S2); XRD patterns of $LaPO_4$, $CePO_4$, and $TbPO_4$ (Figure S3); XRD patterns of the $LaPO_4:Ce^{3+}$ samples obtained at 90 °C for 7.5 h with different amounts of concentrated HNO_3 (Figure S4); XRD patterns of the $LaPO_4:Ce^{3+}$ samples obtained at 90 °C for 7.5 h with different amounts of ethanol (Figure S5); and the simulated crystal structure of hexagonal $LaPO_4$ (Figure S6). This material is available free of charge via the Internet at http://pubs.acs.org